Polymer Solar Cells Based on Quinoxaline and Dialkylthienyl Substituted Benzodithiophene with Enhanced Open Circuit Voltage

Kwan Wook Song, Tae Ho Lee, Eui Jin Ko, Kyung Hun Back, Doo Kyung Moon

Department of Materials Chemistry and Engineering, Konkuk University, 1 Hwayang-dong, Gwangjin-gu, Seoul 143-701, Korea
Correspondence to: D. K. Moon (E-mail: dkmoon@konkuk.ac.kr)

Received 20 September 2013; accepted 19 November 2013; published online 22 January 2014
DOI: 10.1002/pola.27085

ABSTRACT: A poly[benzodithiophene-*alt*-di-2-thienyl-quinoxaline] series (PBDTDPQ-EH, PBDTDPQ-OD, and PBDTDPQ-HDT) was synthesized via Stille coupling. Deep highest occupied molecular orbital (HOMO) levels were achieved by the introduction of 2-decyl-4-hexyl-thiophen-yl (HDT) side chains. The introduction of the various side chains increased the molecular weight of the polymers, and the polymers dissolved well in common organic solvents at room temperature. The HOMO energy level (−5.20 to −5.49 eV) decreased because of the 2D conjugated structure. X-ray diffraction analysis showed that PBDTDPQ-OD had a slightly edge-on structure. In the case of PBDTDPQ-HDT, however, the structure was amorphous due to the thiophene side chain, and the extent of π stacking increased. After fabricating bulk-heterojunction-type polymer solar cells, the OPV characteristics were evaluated. The values of open-circuit voltage (V_{oc}), short-circuit current (J_{sc}), fill factor, and power conversion efficiency (PCE) were 0.88 V, 7.9 mA cm^{-2}, 45.4%, and 3.2%, respectively. © 2014 Wiley Periodicals, Inc. J. Polym. Sci., Part A: Polym. Chem. **2014**, *52*, 1028–1036

KEYWORDS: conjugated polymer; charge transfer; renewable resource; 2D-conjugated structure; quinoxaline; Stille coupling reaction

INTRODUCTION Interest in the development of bulk-heterojunction (BHJ) polymer solar cells (PSCs) is driven by their adaptability to the fabrication of large panels at a low price via the roll-to-roll process. Optimization of the molecular structure of PSCs is important for the realization of high photovoltaic performance.[1,2] The performance of PSCs is governed primarily by the open circuit voltage (V_{oc}), short circuit current density (J_{sc}), and fill factor (FF).[3,4] Further enhancement of the power conversion efficiency (PCE) of PSCs may be achieved by: (1) decreasing the bandgap with an enlarged absorption region, (2) lowering the high occupied molecular orbital (HOMO) energy levels to obtain a high V_{oc}, or (3) increasing the polymer molecular weight.[5,6]

The bandgap of a donor polymer can be decreased by introducing an electron-withdrawing moiety into the polymer main chain.[7] Electron-withdrawing units can be classified as weak, medium, or strong acceptors based on their electron-accepting abilities. When a strong acceptor and medium donor were introduced to the main chain, polymers had good donor–acceptor (D–A) orbital mixing.[8] Benzo[1,2-b:4,5-b′]dithiophene (BDT) has been widely utilized in PSCs as a medium electron-donating unit because of its low intramolecular rotation, face-to-face π stacking, and good charge transfer properties. Its rigid and coplanar structure gives rise to efficient conjugation, and the absorption region is expanded to long wavelengths. However, polymers containing BDT typically have high HOMO levels, resulting in a low oxidative stability. A reduction in the HOMO level of BDT-containing polymers has been attempted by the introduction of a 2D conjugated structure. Hou et al. first proposed a polymer containing new benzodithiophene moiety based on a dialkyl thiophene side chain, which was characterized by a deep HOMO level (−5.31 eV).[9] Since then, Min et al. suggested a conjugated side chain isolation in the copolymer, that is, a 2D conjugated structure, using an alkyl thiophene unit as a side chain.[10] The polymer exhibited better thermal stability, red-shifted absorption spectra, lower HOMO levels, significantly higher hole mobilities, and greatly improved photovoltaic properties. Despite these merits, the reduction of HOMO levels is still not facile.[11] It is difficult to increase the V_{oc} because of the high HOMO energy level of the polymer. Li and coworkers demonstrated a HOMO energy level of −5.13 and −5.26 eV, and a V_{oc} of 0.60 and 073 V.[10] Yang and coworkers presented a V_{oc} of 0.74 V.[12] Thus, an electron acceptor was chosen carefully to obtain a high V_{oc}.[13] As a result, Stefan and coworkers reported that the polymer showed a V_{oc} of 1.04 V with a 3,3′,5-trihexylbithienyl side chain and a 5-hexylthieno[3,4-c]pyrrole-4,6-dione as an electron acceptor.[14]

Additional Supporting Information may be found in the online version of this article.

Quinoxaline moieties act as strong acceptors due to the presence of two imine nitrogen atoms.[8,15] However, the limited solubility of quinoxaline necessitates the introduction of a side chain, with consequent alteration of the electronic properties of the synthesized polymers.[15,16] Andersson and coworkers and Kitazawa et al. reported on the effects of introducing various types of substituents at the 2,3-positions of quinoxaline, demonstrating that the introduction of a phenyl unit at these positions gave rise to the lowest energy bandgap of the polymer.[17,18] Despite the low solubility of alkoxy chainless quinoxaline units, the polymer containing quinoxaline showed an excellent PCE (5.5% in mixed chlorobenzene and chloroform) compared to the APFO-15 (PCE: 3.7%) demonstrated by Andersson and coworkers.[19,20] Despite the presence of two phenyl rings, an FF value of over 50% was observed. This was because the two phenyl groups of quinoxaline were twisted due to steric hindrance. Thus, it was difficult to exclude phenyl-C71-butyric acid methyl ester (PCBM). The small domain between the donor polymer and the PCBM acceptor was confirmed.[18]

In this study, D–π–A polymers were synthesized using BDT derivatives (a medium donor) and a quinoxaline moiety (a strong acceptor), in which phenyl groups were introduced at the 2,3-positions, in order to enhance the miscibility with PCBM. The type and length of BDT moieties were varied in these polymers, giving rise to deep HOMO energy levels (-5.49 eV) and a high V_{oc} (0.88 V) derived from the 2D conjugated structure.

EXPERIMENTAL

Instruments and Characterization

Unless otherwise specified, all reactions were carried out under nitrogen atmosphere. The solvents were dried by standard procedures. All column chromatography experiments were performed with the use of silica gel (230–400 mesh, Merck) as the stationary phase.^{1}H NMR spectra were acquired on a Bruker ARX 400 spectrometer using $CDCl_3$ solutions, and chemical shifts were recorded in ppm units with TMS as the internal standard. Elemental analyses were performed with an EA1112 unit using a CE instrument. The absorption spectra were acquired in chloroform using a HP Agilent 8453 UV–visible (UV–vis) spectrophotometer. Cyclic voltammetry experiments were performed with a Zahner IM6eX Potentionstat/Galvanostat. All measurements were carried out at room temperature with a conventional three-electrode configuration consisting of platinum working and auxiliary electrodes, and a nonaqueous Ag/AgCl reference electrode, at a scan rate of 100 mV s^{-1}. Acetonitrile was used as the solvent in all experiments, and the supporting electrolyte was 0.1 M tetrabutyl ammonium hexafluorophosphate (n-Bu_4NPF_6). X-ray diffraction (XRD) patterns were obtained using a New D8-Advance (Bruker-AXS) instrument. Theoretical analysis was performed using density functional theory (DFT) as approximated by the B3LYP functional, and the 6–31G(d) basis set in Gaussian09. The current–voltage (J–V) curves of the photovoltaic devices were measured using a computer-controlled Keithley 2400 source measurement unit (SMU) that was equipped with a Peccell solar simulator, under AM 1.5 G illumination (100 mW cm^{-2}). Topographic images of the active layers were obtained via atomic force microscopy (AFM) in tapping mode, under ambient conditions, using an XE-100 instrument. Transmission electron microscopy (TEM) was performed using a JEOL 2100F instrument at an accelerating voltage of 200 kV.

Fabrication and Characterization of PSCs

All the BHJ photovoltaics (PV) cells were prepared using the following device fabrication procedure. Indium tin oxide (ITO) glass (10 Ω/sq, Samsung corning) was sequentially sonicated in detergent (Alconox in deionized water, 10%), acetone, isopropyl alcohol, and deionized water for a period of 20 min. The moisture was thoroughly removed with a N_2 gas flow. To ensure the complete removal of the remaining water, the ITO glass was heated on a hot plate for 10 min at 100 °C. For the hydrophilic treatment of the ITO glass surface, the glass was cleaned for 10 min in a UVO cleaner, and poly(3,4-ethylene-dioxythiophene):poly(styrene-sulfonate) (PEDOT:PS S, Baytron P 4083 Bayer AG) was passed through a 0.45-μm filter before being deposited onto the ITO glass to produce a 50-nm-thick layer by spin-coating at 4000 rpm. The coated glass was then dried at 120 °C for 20 min inside a glove box. Composite solutions of the polymer and $PC_{71}BM$ were prepared using o-dichlorobenzene (o-DCB). The solutions were filtered through a 0.45-μm polytetrafluoroethylene (PTFE) filter and then spin-coated (1000–4000 rpm, 30 s) on top of the PEDOT:PSS layer. The device fabrication was completed by depositing thin layers of BaF_2 (2 nm), Ba (2 nm), and Al (100 nm) at pressures of less than 10^{-6} Torr. The active area of the device was 0.04 cm^2. Finally, the cell was encapsulated using a UV-curing glue (Nagase, Japan). All devices were fabricated with the following structure: ITO glass/PEDOT:PSS/polymer:PCBM/BaF_2/Ba/Al. The output photocurrent was adjusted to match the photocurrent of the Si reference cell to obtain a power density of 100 mW cm^{-2}. After encapsulation, all devices were operated under ambient atmosphere at 25 °C.

Synthesis

All reagents were purchased from Aldrich, Acros, or TCI. All chemicals were used without further purification. Benzo[1,2-b:4,5-b′]dithiophen-4,8-dione (1), 2,6-bis(trimethyltin)-4,8-di-(2-ethylhexyloxy)benzo[1,2-b:4,5-b′]dithiophene (2), 2,6-bis (trimethyltin)-4,8-di-(2-octyldodecyloxy)benzo[1,2-b:4,5-b′]di thiophene (3), 4-hexyl-2-decyl-thiophene, and 2,6-bis(tri methyltin)-4,8-di-(4-hexyl-2-decyl-thiophen-5-yl)benzo[1,2-b: 4,5-b′]dithiophene (4), and 5,8-bis(5-bromothiophen-2-yl)-2,3-diphenylquinoxaline were synthesized using procedures modified from the literature.[9,18,20–22]

2,6-bis(trimethylltin)-4,8-di-(4-hexyl-2-decyl-thiophen-5-yl)benzo[1,2-b:4,5-b′]dithiophene(4)

4,8-Bis(2-decyl-4-hexyl-2-thienyl)-benzo[1,2-b:4,5-b′]dithiophene (4.2 g, 5.23 mmol) in THF (12 mL) was cooled to -78 °C, and 1.6 M n-butyllithium in hexane (8.2 mL, 13.08 mmol) was

added dropwise. The mixture was stirred for 1 h at the same temperature, and 1.0 M trimethyltin chloride in THF (15.7 mL, 15.74 mmol) was then added dropwise. The mixture was slowly heated to room temperature and stirred overnight. The mixture was quenched with water and then extracted with dichloromethane. The organic layer was dried over Na_2SO_4 and evaporated to produce the yellow viscous product with a yield of 92.8% (5.48 g). ^{1}H NMR($CDCl_3$, 400 MHz, δ/ppm): 7.25–7.24(d, 2H), 6.8(s, 2H), 2.9–2.81(m, 4H), 2.39–2.31(m, 4H), 1.81–1.73(m, 4H), 1.48–1.43 (br, 10H), 1.35–1.28 (br, 34H), 1.11–1.06 (m, 12H), 0.43–0.28 (t, 18H). Anal. calcd. for $C_{56}H_{90}S_4Sn_2$: C 59.58, H 8.03, S 11.36; found: C 58.95, H 7.93, S 10.34.

General Polymerization

Representative Procedure for Polymerization: Polymerization of Poly[(4,8-di-(4′-hexyl-2′-decyl-thiophen-5′-yl)benzo[1,2-b:4,5-b′]dithiophene-2,6-diyl)-alt-5,8-bis(5′-thiophen-2-diyl)-2,3-diphenylquinoxaline)], PBDTDTQ-HDT

5,8-Bis(5-bromothiophen-2-yl)-2,3-diphenylquinoxaline (18 1.3 mg, 0.3 mmol) and tri(*o*-tolyl)phosphine (14.6 mg, 0.048 mmol) were dissolved in toluene (28 mL). The flask was degassed and refilled with nitrogen gas twice, and then 2,6-bis(trimethyltin)-4,8-di(2-decyl-4-hexyl-2-thienyl)-benzo [1,2-b:4,5-b′]dithiophene (338.7 mg, 0.3 mmol) and tris(dibenzylideneacetone)dipalladium(0) (10.98 mg, 0.012 mmol) were added to the mixture. The flask was degassed and refilled twice. The polymerization mixture was stirred at 110 °C for 48 h, and a few drops of 2-bromothiophene were added. After 3 min, a few drops of 2-tributylstannyl thiophene were also added for the end-capping reaction. The reaction mixture was cooled to room temperature and poured into methanol. The precipitate was filtered and purified with methanol, acetone, hexane, and chloroform in a Soxhlet apparatus. The polymer was washed with ethylenediamine tetraacetic acid (EDTA) and water, then extracted with solid phase extraction (SPE) and precipitated in methanol. Finally, the polymer was collected as a solid (60%, 229.9 mg) ^{1}H NMR($CDCl_3$, 400 MHz, δ/ppm): 8.2–7.9 (br, 2H), 7.9–7.5 (br, 8H), 7.5–7.2 (br, 6H), 7.2–7.1 (br, 2H), 7.1–6.8 (br, 2H), 3.2–2.8 (br, 4H), 2.6–2.2 (br, 4H), 2.0–1.8 (br, 4H), 1.8–1.2 (br, 44H), 1.2–1.0 (br, 12H). Anal. calcd. for $C_{78}H_{90}N_2S_6$: C 75.07, H 7.27, N 2.24, S 15.42; found: C 73.36, H 7.16, N 2.20, S 14.0.

PBDTDPQ-EH and PBDTDPQ-OD were synthesized according to the same procedure used for PBDTDTQ-HDT with the relevant monomers. ^{1}H NMR, gel permeation chromatography (GPC) data, and elemental analysis for the polymers are presented, except for elemental analysis of PBDTDPQ-EH due to low yield.

PBDTDPQ-EH.

19%, 50 mg, ^{1}H NMR($CDCl_3$, 400 MHz, δ/ppm): 7.9–7.5 (br, 8H), 7.5–7.2 (br, 6H), 7.2–7.1 (br, 2H), 7.1–6.8 (br, 2H), 4.3–3.9 (br, 4H), 2.0–1.8 (br, 2H), 1.8–1.2 (br, 12H), 1.2–1.0 (br, 12H).

PBDTDPQ-OD.

83%, 302 mg, ^{1}H NMR($CDCl_3$, 400 MHz, δ/ppm): 7.9–7.5 (br, 8H), 7.5–7.2 (br, 6H), 7.2–7.1 (br, 2H), 7.1–6.8 (br, 2H), 4.3–3.9 (br, 4H), 2.0–1.8 (br, 2H), 1.8–1.2 (br, 64H), 1.2–1.0 (br, 12H). Anal. calcd. for $C_{76}H_{100}N_2O_2S_4$: C 75.95, H 8.39, N 2.33, O 2.66, S 10.67; found: C 75.97, H 8.39, N 2.16, O 2.88, S 10.17.

RESULTS AND DISCUSSION

Polymer Synthesis

Scheme 1 shows the general synthetic routes for each polymer. Three types of benzodithiophene derivatives and quinoxaline units were used for the synthesis. The polymers were synthesized via a palladium-catalyzed Stille coupling reaction at 100 °C for 48 h, using toluene and Pd(0) as the solvent and catalyst, respectively. At the end of the polymerization, the mixture was end-capped by the sequential addition of 2-bromothiophene and 2-tributyl stannyl thiophene. The mixture was then reprecipitated by adding methanol, and a black powder was obtained. The obtained powders were purified by sequential treatment with methanol, acetone, hexane, and chloroform using a Soxhlet apparatus. Finally, the chloroform-soluble portion was reprecipitated in methanol. The obtained polymers dissolved readily in tetrahydrofuran (THF), chlorobenzene, and *o*-DCB. The structures were analyzed using ^{1}H NMR. Supporting Information Figure S1 shows data confirming the successful synthesis of the poly[benzodithiophene-*alt*-di-2-thienyl-quinoxaline] series (PBDTDPQ-EH, PBDTDPQ-OD, and PBDTDPQ-HDT). The number-average molecular weights (M_n) of the synthesized polymers were 9.8 kg mol^{-1} for PBDTDPQ-EH, 24.3 kg mol^{-1} for PBDTDPQ-OD, and 20.0 kg mol^{-1} for PBDTDPQ-HDT. The polydispersity indexes (PDIs) were determined to be 1.55, 2.86, and 1.88, respectively.

Optical and Electrochemical Properties

Figure 1 shows the UV–vis absorption spectra of the polymer solutions in chloroform and of the films on a quartz plate. For PBDTDPQ-EH and PBDTDPQ-OD, both of which have a branched alkoxy chain in the DBT unit, two similar absorption peaks were observed in both the solution and film. In the case of PBDTDPQ-EH, absorption peaks were detected at 406 and 555 nm for the solution and at 431 and 583 nm for the film. In the case of PBDTDPQ-OD, absorption peaks were found at 413 and 576 nm in solution and at 423 and 589 nm in the film state.

However, in the case of PBDTDPQ-HDT, which has a thiophene side chain in the BDT unit, three absorption peaks were detected both in the solution (337, 404, and 544 nm) and film (342, 418, and 568 nm) states. In particular, the absorption peak around 340 nm was attributed to the thiophene side chain and was distinguishable from the other two polymers. Similar results have been reported in other studies of polymers with a 2D structure.[9,11,23,24] The absorption peaks of the three polymers were red-shifted in solution relative to the solid. Increasing the length of the alkoxy chain from ethyl hexyl to octyl dodecyl also produced a slight red shift in the absorption spectra. These shifts were attributed to the improved solubility of the polymers with the extended side chains and stable interaction among the polymers. In contrast, the absorption spectra of the thiophene side-chain-

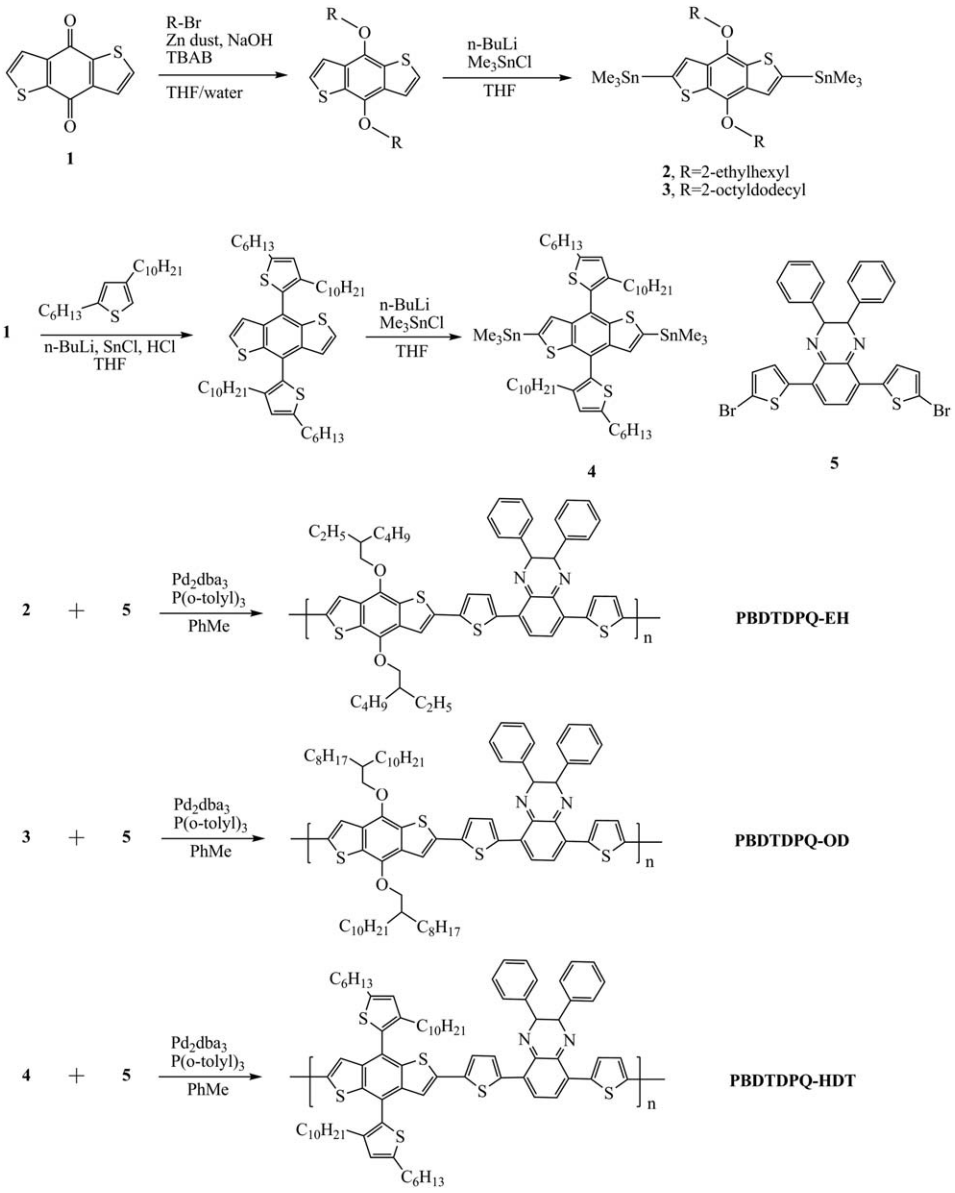

SCHEME 1 The synthesis of monomers and polymers.

appended PBDTDPQ-HDT species were slightly blue-shifted. The bandgap of the polymer increased to 1.81 eV. Similar behavior, in which the thiophene side chain decreased only the HOMO level, was reported by Yang and coworkers, regardless of the energy of the lowest unoccupied molecule orbital (LUMO) level.[12,22]

Figure 1(c) and Table 1 show the cyclic voltammograms of the three polymers, measured using 0.1 M tetrabutylammonium-hexafluorophosphate (n-Bu_4PF_6) in the acetonitrile solution. The oxidation onsets (E_{ox}^{onset}) for the alkoxy chain-based PBDTDPQ-EH and PBDTDPQ-OD were 0.86 and 0.92 V, and the HOMO energy levels were calculated to be −5.20 and −5.26 eV, respectively. The octyl dodecyl chain-based PBDTDPQ-OD had a relatively low HOMO level. In contrast, the HOMO level of PBDTDPQ-HDT, to which the thiophene side chain was introduced, decreased to −5.49 eV. This decrease in the HOMO level of the 2D conjugated polymer with the thiophene side chain was attributed to the extended delocalized electron density,[10] which was consistent with observations by Hou et al.[1] The LUMO levels of PBDTDPQ-EH, PBDTDPQ-OD, and PBDTDPQ-HDT were calculated as −3.47, −3.52, and −3.68 eV, respectively, based on the differences between the optical bandgap of the polymers and the HOMO levels. Although the bandgaps of the three polymers were similar, the LUMO level of PBDTDPQ-HDT was the lowest due to the reduction of the HOMO level by the introduction of the thiophene chain.

Computational Study

The molecular geometries and electron density of states distribution of the polymers were simulated using DFT to

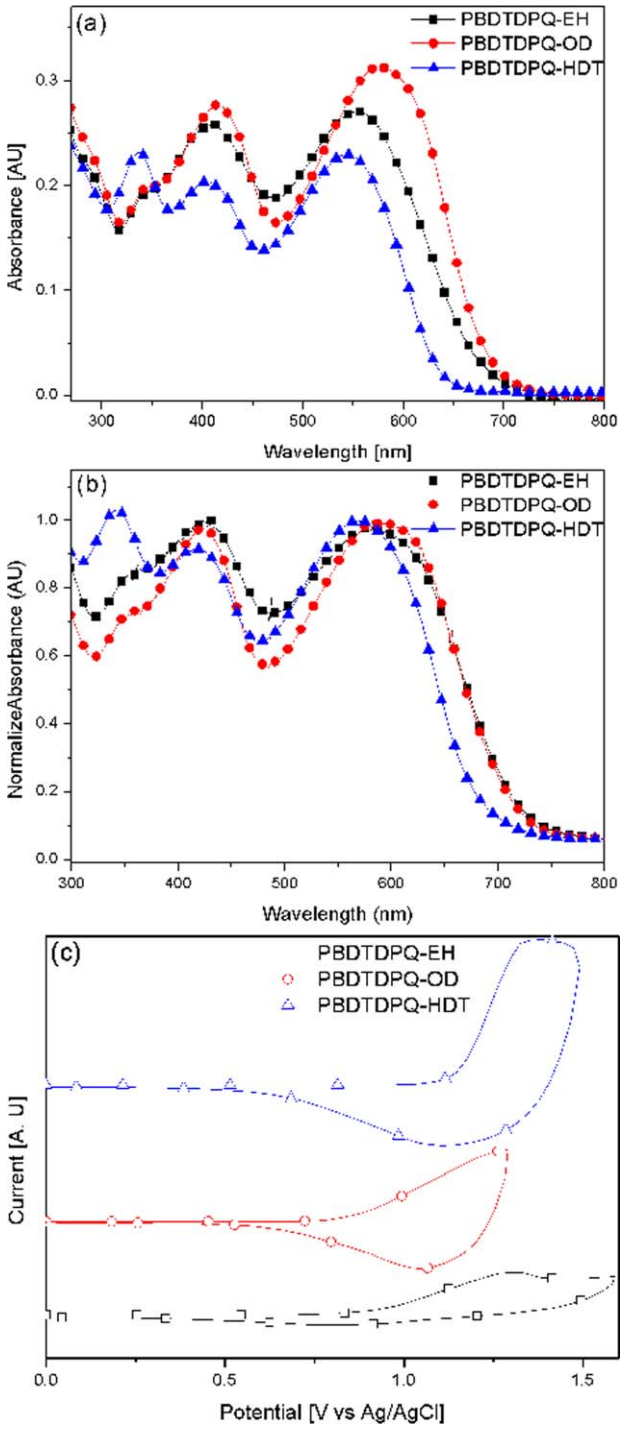

FIGURE 1 Absorption spectra of PBDTDPQ-EH, PBDTDPQ-OD, and PBDTDPQ-HDT in (a) chloroform solution and (b) film state; (c) cyclic voltammograms of the polymer films on ITO electrodes in a 0.1 mol L^{-1} n-Bu_4NPF_6 acetonitrile solution; sweep rate: 100 mV s^{-1}. [Color figure can be viewed in the online issue, which is available at wileyonlinelibrary.com.]

investigate electronic properties. DFT calculations were performed using Gaussian 09 based on the hybrid B3LYP correlation functional and split valence 6-31G(d) basis set.[6,25] Oligomers, which have two repeat units, were selected as a calculation model. Branch and thiophene chains were simplified into a 2-propyl methyl oxy group and two methyl groups, respectively. Figure 2 shows the calculated HOMO and LUMO orbitals. As measured in the cyclic voltammogram, a HOMO level (−4.76 eV) of PBDTDPQ-HDT was relatively low because of the extension of delocalized molecular orbitals by 2D conjugation. The thiophene side chain was tilted in the main chain due to the interaction between the sulfur atoms, as also observed in previous studies.[1,24] Supporting Information Figure S2 shows the relative energy difference of thienyl benzodithiohene as a function of the dihedral angle. The thiophene side chain was stable when the tilted angle of the benzodithiophene unit was in the range of 60–120°. As a result, the side chain of PBDTDPQ-HDT formed a "sticking-out" conformation, which was placed vertically on the main chain.[26] The distance between the side chain of BDT and the phenyl ring of quinoxaline increased from 6 Å to ∼10 Å, and the free volume of PBDTDPQ-HDT was enlarged.

McGehee and coworkers reported that fullerene intercalation is likely to occur in blends with both amorphous and semicrystalline polymers when there is enough free volume between the side chains to accommodate the fullerene molecule.[27] Therefore, the contact channel with PCBM might increase because of the enlarged free volume.

XRD Measurement

Figure 3 shows XRD patterns of the polymers and polymer: PCBM samples. The two studied polymers were structural isomers, with only a small difference in the shape of the alkyl chains attached to BDT (branched 2-ethylhexane vs straight hexyldecyl thiophene). In the case of out-of-plane PBDTDPQ-OD, sharp diffraction peaks were observed at 4.16° and 7.20°, indicating the formation of ordered (100) and lamellar (200) structures. Using Bragg's law ($\lambda = 2d\sin\theta$), the lamellar d-spacing (d_1) was determined to be 21.2 Å.

The appearance of the (200) peak further confirmed that the polymer chain was interdigitated. The π–π stacking distance (d_π) of PBDTDPQ-OD was 3.75 Å ($2\theta = 23.7°$). In contrast, PBDTDPQ-OD was mostly amorphous with a partially mixed edge-on and face-on crystalline structure. In the case of PBDTDPQ-HDT, the crystallinity was decreased by the thiophene side chain due to the tilted dihedral angle of the 2D conjugated structure.[1,24] The d_π spacing increased to 3.94 Å ($2\theta = 22.5°$). Depending upon the linkage component of the side chains, the change in the crystallinity of the polymers was first confirmed via XRD. Introducing the thiophene side chain caused the ordered polymers to become amorphous, and increased the d_π. The peaks from PBDTDPQ-OD:PCBM blended film were similar to a corresponding peak of PBDTDPQ-OD, except for the peak of PCBM near 18°.[28,29] However, the intensity of the peaks corresponding to the d_π was reduced in the XRD pattern of PBDTDPQ-HDT:$PC_{71}BM$. It was buried by the peak of PCBM.[29] This barely-discernible

TABLE 1 Molecular Weights and Physicochemical Properties of Polymers.

Polymer	M_n[a] (kg mol^{-1})[a]	PDI[b]	λ_{onset} (nm)	E_g^{opt} (eV)[c]	HOMO (eV)	LUMO (eV)[d]
PBDTDTQ-EH	9.8	1.55	716	1.73	−5.20	−3.47
PBDTDTQ-OD	24.3	2.86	713	1.74	−5.26	−3.52
PBDTDTQ-HDT	20.0	1.88	682	1.81	−5.49	−3.68

[a] Determined via GPC in THF using polystyrene standards.
[b] Calculated values in which M_n is divided by the molecular weight of repeating units.
[c] Calculated from the intersection of the tangent on the low energetic edge of the absorption spectrum with the baseline.
[d] LUMO = HOMO + E_g^{opt}.

(010) peak indicated a less planar structure and, consequently, decreased intermolecular packing.

Photovoltaic Properties

BHJ PSCs were fabricated to determine the photovoltaic properties arising from the 2D conjugated chain. Figure 4(a) shows the *J–V* curve of the BHJ PSCs, and Figure 4(b) shows the incident photon-to-current efficiency (IPCE). The photovoltaic properties of all polymers were evaluated after fabricating ITO/PEDOT:PSS/polymer: $PC_{71}BM$/BaF_2/Ba/Al-structured PSC devices. The fabricated devices were then encapsulated under controlled conditions in a glove box. The *J–V* characteristics of the devices were measured for an active area of 0.04 cm^2 under ambient atmosphere. Table 2 summarizes the photovoltaic properties of the fabricated PSCs. Despite the short side chain, PBDTDPQ-EH had an FF of 50.6%, but the V_{oc} (0.56 V) was very low, with a PCE of 1.1%. However, PBDTDPQ-OD, with a long octyl dodecyl side chain, had a HOMO level lower than that of PBDTDPQ-EH. Thus, the V_{oc} (0.79 V) was enhanced. The largest shunt resistance (R_{sh}), an improved FF (57.5 %), and a PCE of 1.6% were observed. In contrast, because PBDTDPQ-HDT has a 2D structure, a wider delocalized molecular orbital and a larger interface with PCBM were detected, giving rise to the largest V_{oc} (0.88 V), J_{sc} (7.9 mA cm^{-2}), and PCE (3.2%).

However, the long side chain and tilted nature of the thiophene caused declines in R_{sh} and FF. As the length of the side chain increased, both the V_{oc} and the FF increased. With the introduction of the 2D conjugated structure, J_{sc} almost doubled, with a consequent increase in the PCE.

Figure 4(b) shows the external quantum efficiency (EQE) of the polymers. The IPCE of the three polymers was within the absorption range of 300–700 nm. In particular, PBDTDPQ-HDT, which had the highest J_{sc}, showed the largest conversion efficiency of 55% at 440 nm. To optimize photovoltaic performance, Supporting Information Figure S3 shows the *J–V* and the IPCE curve of PBDTDPQ-OD and -HDT.

Morphology Analysis

The morphology of the polymer/$PC_{71}BM$ blend film was evaluated using AFM and transmittance electron microscopy (TEM), as shown in Figure 5. Figure 5(a,b) shows the height image and the phase image of the PBDTDPQ-OD/$PC_{71}BM$ blend film. As shown in Figure 5(a), the root mean square (RMS) roughness of PBDTDPQ-OD was measured to be 3.78 nm. The surface roughness indicated the ordering of the polymer self-organization.[30] As shown in Figure 5(b), micro-

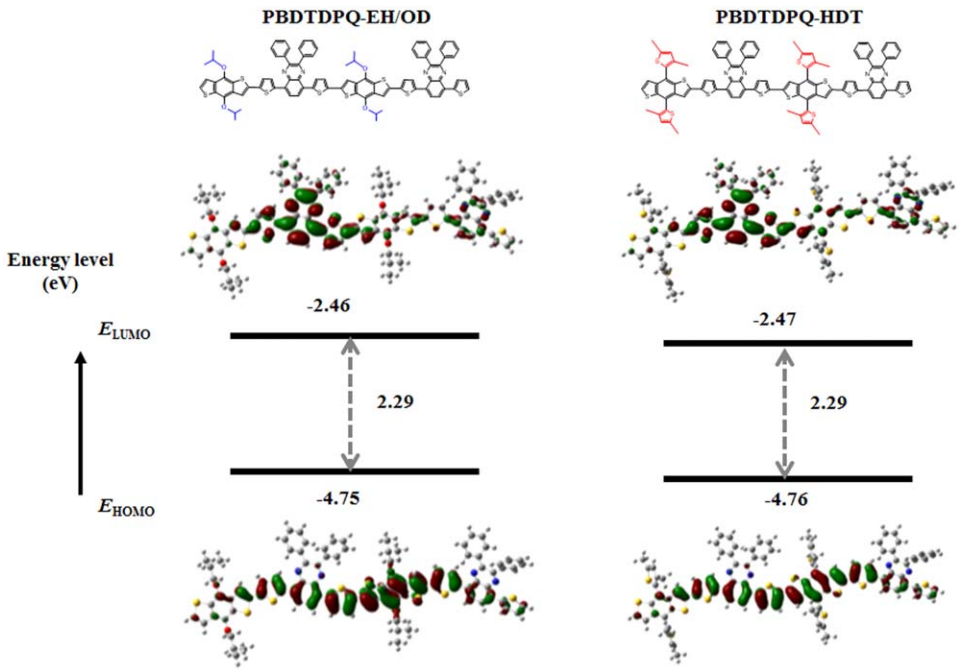

FIGURE 2 The Gaussian calculation of polymer energy levels. [Color figure can be viewed in the online issue, which is available at wileyonlinelibrary.com.]

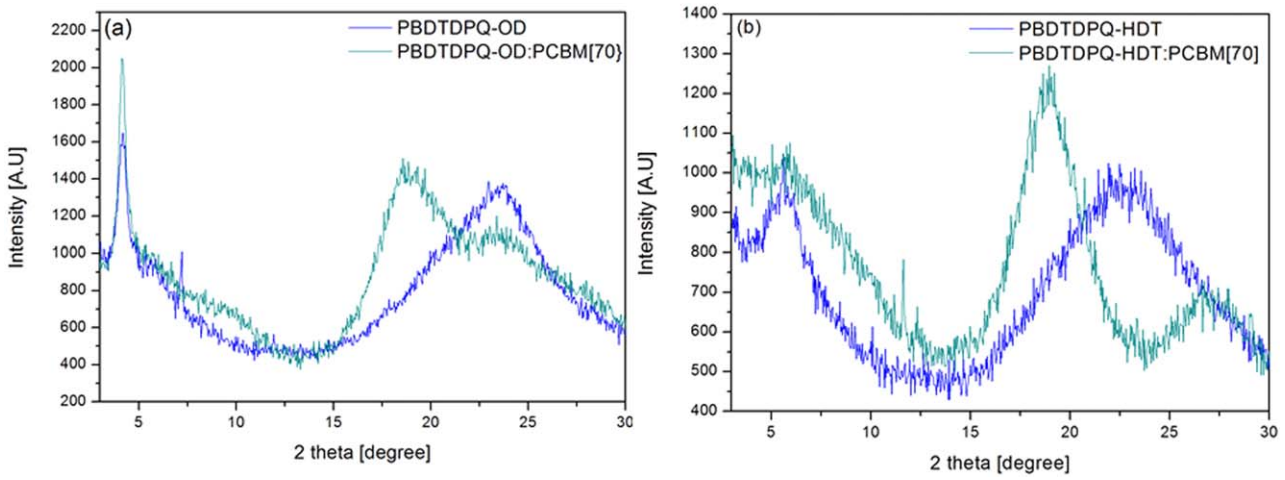

FIGURE 3 XRD patterns of polymers and polymer: PCBM. [Color figure can be viewed in the online issue, which is available at wileyonlinelibrary.com.]

scale phase separation was also observed in the phase image. The TEM image in Figure 5(c) showed that a 100-nm PCBM domain was formed, which was greater than the organic exciton diffusion length.[1,30] Although PBDTDPQ-OD had an enhanced solubility as compared to PBDTDPQ-EH, only the polymer or PCBM domain formed because of the low J_{sc}.

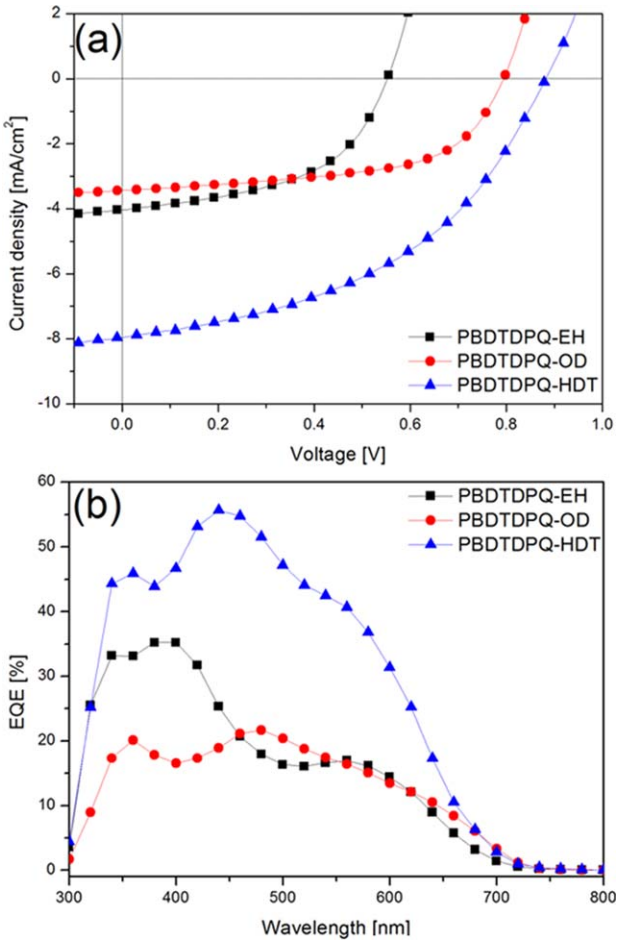

FIGURE 4 (a) The J–V characteristics and (b) IPCE spectra of BHJ solar cells with the device. [Color figure can be viewed in the online issue, which is available at wileyonlinelibrary.com.]

However, as shown in Figure 5(d), PBDTDPQ-HDT had a different height. The RMS roughness of PBDTDPQ-HDT was 0.42 nm. Because of the introduction of the thiophene side chain, the PBDTDPQ-HDT/$PC_{71}BM$ blend film had a smoother morphology and a nano-scaled phase separation, as expected based on Gaussian calculations and XRD measurements. The phase and TEM image of PBDTDPQ-HDT/$PC_{71}BM$ [Fig. 5(e,f)] showed a well-mixed flat layer, and no domain was observed. As shown in the inset of Figure 5(f), the measurement of the dark field STEM showed well-distributed $PC_{71}BM$. Supporting Information Figure S4 shows the morphology of the polymer/$PC_{71}BM$ blend in the 1-μm^2 scale, which confirmed the same results.

CONCLUSIONS

Three different D–π–A polymers of the poly[benzodithiophene-*alt*-di-2-thienyl-quinoxaline] series (PBDTDPQ-EH, PBDTDPQ-OD, and PBDTDPQ-HDT) were synthesized via Stille coupling. Long and thiophene side chains were introduced into these polymers to increase the molecular weight,

TABLE 2 The Photovoltaic Performance of Polymers.

Polymer	PCBM ratio (wt/wt %)	V_{oc} (V)	J_{sc} (mA cm^{-2})	FF (%)	PCE (%)	R_{sh} (Ω cm^2)
PBDTDPQ-EH	1:1	0.56	4.0	50.6	1.1	1010.00
PBDTDPQ-OD	1:1	0.79	3.4	57.5	1.6	2019.99
	1:3	0.78	2.5	65.8	1.3	2084.62
PBDTDPQ-HDT	1:2	0.88	8.0	39.2	2.8	483.09
	1:3	0.88	7.9	45.4	3.2	763.36
	1:4	0.86	8.5	41.5	3.0	381.68

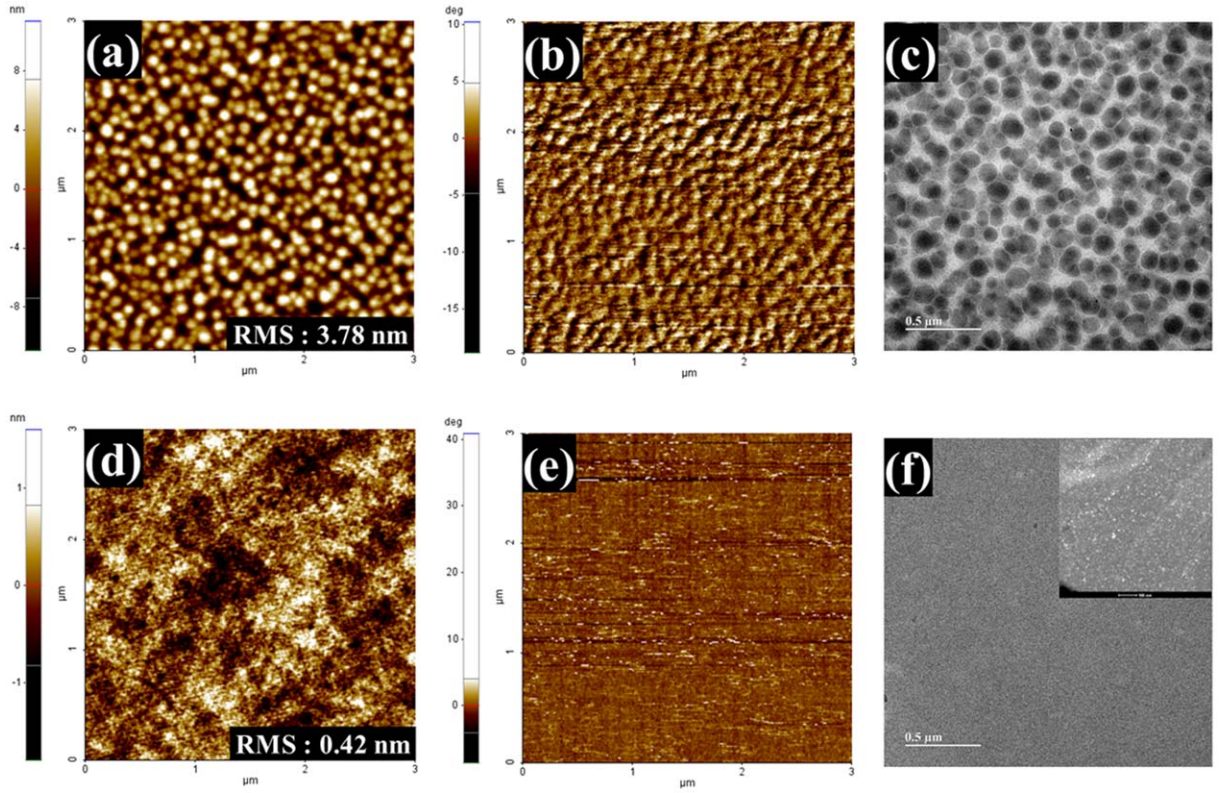

FIGURE 5 Topographic AFM images (a, d), phase images (b, e), and TEM images (c, f) of PBDTDPQ-OD:$PC_{71}BM$ (1:1 wt/wt, 3 × 3 μm^2) (a–c) and PBDTDPQ-HDT:$PC_{71}BM$ (1:3 wt/wt, 3 × 3 μm^2) (d–f), (inset of (f): STEM image). [Color figure can be viewed in the online issue, which is available at wileyonlinelibrary.com.]

lower the HOMO level, and promote mixing with PCBM, respectively. The molecular weights of PBDTDPQ-OD and PBDTDPQ-HDT increased to 24.3 and 20.0 kg mol^{-1}, respectively. The bandgap (1.81 eV) increased for PBDTDPQ-HDT appended with a 2D conjugated side, whereas the HOMO level decreased to −5.49 eV. XRD analysis indicated that the tilted thiophene side chain gave rise to an amorphous structure for PBDTDPQ-HDT. The AFM measurement confirmed the smooth surface and efficient mixing with $PC_{71}BM$. The V_{oc}, J_{sc}, FF, and PCE of PBDTDPQ-HDT were 0.88 V, 7.9 mA cm^{-2}, 45.4%, and 3.2%, respectively.

ACKNOWLEDGMENTS

This research was supported by a grant from the Fundamental R&D Program for Core Technology of Materials, funded by the Ministry of Knowledge Economy, Republic of Korea. This work was also supported by the National Research Foundation of Korea Grant, funded by the Korean Government (MEST) (NRF-2009-C1AAA001-2009-0093526).

REFERENCES AND NOTES

1 L. Huo, L. Ye, Y. Wu, Z. Li, X. Guo, M. Zhang, S. Zhang, J. Hou, *Macromolecules* **2012**, *45*, 6923–6929.

2 R. S. Kularatne, H. D. Magurudeniya, P. Sista, M. C. Biewer, M. C. Stefan, J. *Polym. Sci., Part A: Polym. Chem.* **2013**, *51*, 743–768.

3 P.-L. T. Boudreault, A. Najari, M. Leclerc, *Chem. Mater.* **2011**, *23*, 456–469.

4 A. Moliton, J.-M. Nunzi, *Polym. Int.* **2006**, *55*, 583–600.

5 H.-J. Song, D.-H. Kim, E.-J. Lee, S.-W. Heo, J.-Y. Lee, D.-K. Moon, *Macromolecules* **2012**, *45*, 7815–7822.

6 K. W. Song, H. J. Song, T. H. Lee, S. W. Heo, D. K. Moon, *Polym. Chem.* **2013**, *4*, 3225–3235.

7 D.-H. Yun, H.-S. Yoo, S.-W. Heo, H.-J. Song, D.-K. Moon, J.-W. Woo, Y.-S. Park, *J. Ind. Eng. Chem.* **2013**, *19*, 421–426.

8 Z. G. Zhang, J. Wang, *J. Mater. Chem.* **2012**, *22*, 4178–4187.

9 L. Huo, J. Hou, S. Zhang, H.-Y. Chen, Y. Yang, *Angew. Chem. Int. Ed.* **2010**, *49*, 1500–1503.

10 J. Min, Z.-G. Zhang, S. Zhang, Y. Li, *Chem. Mater.* **2012**, *24*, 3247–3254.

11 R. Duan, L. Ye, X. Guo, Y. Huang, P. Wang, S. Zhang, J. Zhang, L. Huo, J. Hou, *Macromolecules* **2012**, *45*, 3032–3038.

12 L. Dou, J. You, J. Yang, C.-C. Chen, Y. He, S. Murase, T. Moriarty, K. Emery, G. Li, Y. Yang, *Nat. Photonics* **2012**, *6*, 180–185.

13 L. Bian, E. Zhu, J. Tang, W. Tang, F. Zhang, *Prog. Polym. Sci.* **2012**, *37*, 1292–1331.

14 R. S. Kularatne, P. Sista, H. Q. Nguyen, M. P. Bhatt, M. C. Biewer, M. C. Stefan, *Macromolecules* **2012**, *45*, 7855–7862.

15 H.-J. Song, D.-H. Kim, E.-J. Lee, D.-K. Moon, *J. Mater. Chem. A* **2013**, *1*, 6010–6020.

16 M.-J. Baek, H. Park, P. Dutta, W.-H. Lee, I.-N. Kang, S.-H. Lee, *J. Polym. Sci. Part A: Polym. Chem.* **2013**, *51*, 1843–1851.

17 L. J. Lindgren, F. Zhang, M. Andersson, S. Barrau, S. Hellström, W. Mammo, E. Perzon, O. Inganäs, M. R. Andersson, *Chem. Mater.* **2009**, *21*, 3491–3502.

18 D. Kitazawa, N. Watanabe, S. Yamamoto, J. Tsukamoto, *Sol. Energy Mater. Sol. Cells* **2012**, *98*, 203–207.

19 A. Gadisa, W. Mammo, L. M. Andersson, S. Admassie, F. Zhang, M. R. Andersson, O. Inganäs, *Adv. Funct. Mater.* **2007**, *17*, 3836–3842.

20 D. Kitazawa, N. Watanabe, S. Yamamoto, J. Tsukamoto, *Appl. Phys. Lett.* **2009**, *95*, 053701.

21 J. Hou, M.-H. Park, S. Zhang, Y. Yao, L.-M. Chen, J.-H. Li, Y. Yang, *Macromolecules* **2008**, *41*, 6012–6018.

22 L. Huo, J. Hou, H.-Y. Chen, S. Zhang, Y. Jiang, T. L. Chen, Y. Yang, *Macromolecules* **2009**, *42*, 6564–6571.

23 L. Huo, S. Zhang, X. Guo, F. Xu, Y. Li, J. Hou, *Angew. Chem. Int. Ed.* **2011**, *50*, 9697–9702.

24 J. Yuan, Z. Zhai, H. Dong, J. Li, Z. Jiang, Y. Li, W. Ma, *Adv. Funct. Mater.* **2013**, *23*, 885–892.

25 K. W. Song, M. H. Choi, J. Y. Lee, D. K. Moon, *J. Ind. Eng. Chem.* **2014**, *1*, 290–296.

26 J. Liu, H. Choi, J. Y. Kim, C. Bailey, M. Durstock, L. Dai, *Adv. Mater.* **2012**, *24*, 538–542.

27 A. C. Mayer, M. F. Toney, S. R. Scully, J. Rivnay, C. J. Brabec, M. Scharber, M. Koppe, M. Heeney, I. McCulloch, M. D. McGehee, *Adv. Funct. Mater.* **2009**, *19*, 1173–1179.

28 R. Mens, S. Chambon, S. Bertho, G. Reggers, B. Ruttens, J. D'Haen, J. Manca, R. Carleer, D. Vanderzande, P. Adriaensens, *Magn. Reson. Chem.* **2011**, *49*, 242–247.

29 L. Yang, H. Zhou, W. You, *J. Phys. Chem. C* **2010**, *114*, 16793–16800.

30 S. W. Heo, K. W. Song, M. H. Choi, H. S. Oh, D. K. Moon, *Sol. Energy Mater. Sol. Cells* **2013**, *114*, 82–88.